JCI The Journal of Clinical Investigation

Lack of Flvcr2 impairs brain angiogenesis without affecting the blood-brain barrier

Nicolas Santander, Carlos Omar Lizama, Eman Meky, Gabriel L. McKinsey, Bongnam Jung, Dean Sheppard, Christer Betsholtz, Thomas D. Arnold

J Clin Invest. 2020. https://doi.org/10.1172/JCI136578.

Research In-Press Preview Angiogenesis Development

Graphical abstract

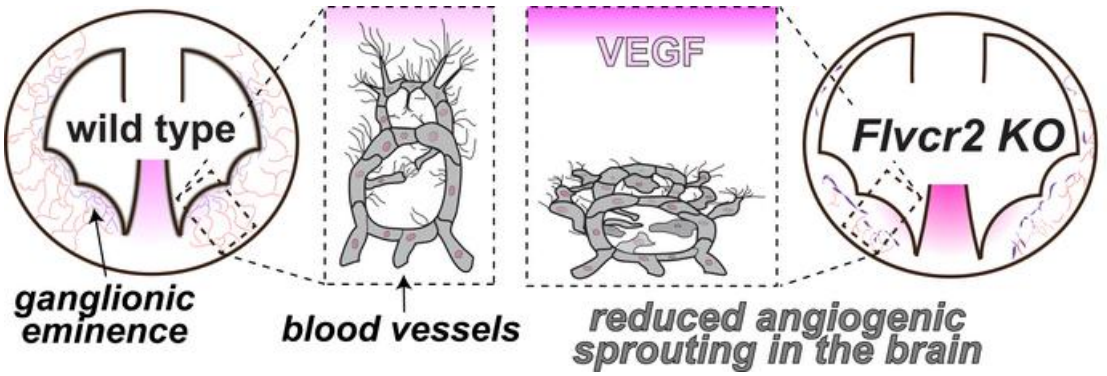

Lack of *Flvcr2* impairs brain angiogenesis without affecting the blood-brain barrier

Nicolas Santander[1], Carlos O. Lizama[2], Eman Meky[1], Gabriel L. McKinsey[1], Bongnam Jung[3], Dean Sheppard[3], Christer Betsholtz[4,5,*], Thomas D. Arnold[1,*].

[1] Department of Pediatrics, University of California San Francisco, USA.

[2] Cardiovascular Research Institute, University of California San Francisco, USA.

[3] Department of Cell Biology, University of California San Francisco, USA.

[4] Integrated Cardiometabolic Center, Department of Medicine Huddinge, Karolinska Institutet, Sweden.

[5] Department of Immunology, Genetics and Pathology, Uppsala University, Sweden.

[*] Co-corresponding authors.

Correspondence to:

Thomas D. Arnold at 1550 Fourth St, 548C, San Francisco, CA 94158. Phone 1-415-476-5153. Thomas.Arnold@ucsf.edu.

Christer Betsholtz at Rudbecklaboratoriet, Uppsala, Sweden 751-85 . Phone 46-018-471-4816. christer.betsholtz@igp.uu.se.

Conflict of interest statement: The authors have declared that no conflict of interest exists.

ABSTRACT

Fowler syndrome is a rare autosomal recessive brain vascular disorder caused by mutation in *FLVCR2* in humans. The disease occurs during a critical period of brain vascular development, is characterized by glomeruloid vasculopathy and hydrocephalus, and is almost invariably prenatally fatal. Here, we sought to gain insights into the process of brain vascularization and the pathogenesis of Fowler Syndrome by inactivating *Flvcr2* in mice. We showed that *Flvcr2* was necessary for angiogenic sprouting in the brain, but surprisingly dispensable for maintaining the blood brain barrier. Endothelial cells lacking *Flvcr2* had altered expression of angiogenic factors, failed to adopt tip-cell properties and displayed reduced sprouting leading to vascular malformations similar to those seen in humans with Fowler Syndrome. Brain hypo-vascularization was associated with hypoxia and tissue infarction, ultimately causing hydrocephalus and death of mutant animals. Strikingly, despite severe vascular anomalies and brain tissue infarction, the blood-brain barrier was maintained in *Flvcr2* mutant mice. Our Fowler syndrome model therefore defined the pathobiology of this disease, and provided new insights into brain angiogenesis by showing uncoupling of vessel morphogenesis and blood-brain barrier formation.

INTRODUCTION

Developmental vascularization, the process by which blood vessels grow into and differentiate within a tissue, is remarkably organ-specific. Cerebral angiogenesis is a foremost example. Here, blood vessels sprout from a primitive perineural plexus into the brain parenchyma, until they reach the lateral ventricles, and then grow laterally to form a secondary plexus spanning the ventricular zone (1). As vessels grow into the brain they coordinately acquire barrier properties (the blood brain barrier, BBB) which are a unique and defining feature of central nervous system (CNS) vasculature. Indeed, mRNA profiling studies reveal significant differences between endothelial cells in the brain versus other organs (2, 3). Many of these "BBB-specific" genes encode transporters or cellular junction proteins, and mouse mutants lacking some of these genes [e.g. *Mfsd2a*, *Lsr*, *Cldn5* (4–6)] have isolated BBB dysfunction. On the other hand, disruption of αVβ8/TGF-β or Wnt/β-Catenin signaling during development produces CNS-specific angiogenic abnormalities and concomitant BBB dysfunction (7, 8), suggesting that downstream programs controlling cerebral angiogenesis and barrier-genesis are overlapping. The genes regulating cerebral angiogenesis independent from the BBB are entirely unknown; to the best of our knowledge there are as yet no mouse models that display abnormal vascular growth and, at the same time, an intact BBB. The discovery of such a model would be immensely useful in understanding how vascular growth and differentiation is specifically regulated in the CNS, and could help determine the downstream consequences of abnormal CNS angiogenesis versus BBB dysfunction.

In humans, mutations in the poorly studied gene *FLVCR2* (also known as *MFSD7C, SLC49A2,* and *CCT*) underlie the development of proliferative vasculopathy with hydranencephaly-hydrocephaly syndrome (PVHH; OMIM 225790), also known as Fowler

syndrome (9). This gene is part of the major facilitator superfamily and has been proposed as a putative heme importer (10, 11). Its expression is restricted to brain endothelial cells (3), suggesting a role in the barrier properties of these cells.

PVHH is an autosomal recessive prenatal lethal disorder characterized by severe hydrocephalus and thin cerebral cortex, glomeruloid vascular structures in the brain, and diffuse ischemic lesions in the brain stem and embryonic basal ganglia or ganglionic eminence (GE) (12). To date, there are 16 different reported *FLVCR2* mutations in humans: one large deletion, two nonsense mutations, one splice-site mutation, one insertion/deletion change, and 11 missense variations (9, 13, 14). These are most likely loss-of-function mutations since heterozygotes are not normally affected, and because most affected individuals are compound heterozygotes, having two different recessive alleles at the *FLVCR2* locus. While the exact consequences of these mutations have not yet been tested in existing functional assays (11), multiple sequence alignment and homology modeling support local conformational changes (usually affecting transmembrane domains with predicted dysfunction of the channel) or reduced expression (null mutations) (13). Furthermore, in the genome aggregation database (gnomAD, gnomad.broadinstitute.org), no homozygous loss-of-function mutation is reported in the *FLVCR2* locus in over 125,000 exomes and 15,000 genomes from adults, again suggesting that loss-of-function mutations (and not potentially activating mutations) are responsible for PVHH. Due to the rarity of the syndrome and the lack of a good animal model, the step-wise progression of vascular abnormalities, hydrocephalus and embryonic lethality, and the contribution of BBB dysfunction to this pathology, is not known.

Here, we have generated a mouse model of PVHH by inactivating mouse *Flvcr2* in an effort to better understand brain vascular and BBB co-development, and to deconstruct the

molecular pathophysiology of this disease. We show that *Flvcr2* is specifically expressed in CNS endothelial cells throughout development and into adulthood, and that inactivation of *Flvcr2* in these cells severely impairs brain vascular growth. Surprisingly, knockout mice have an intact BBB, suggesting that the downstream phenotypes observed in mice and humans with mutant *FLVCR2* (hydrocephalus and embryonic lethality), are a consequence of abnormal brain angiogenesis and not BBB dysfunction. These observations disentangle the co-development of the BBB and brain blood vessels, and describe distinct downstream consequences of impaired vascular growth in the brain.

RESULTS

Flvcr2 is selectively expressed in CNS endothelium and pericytes.

Proliferative Vasculopathy, Hydrocephaly-Hydranencephaly Syndrome (PVHH) is a rare autosomal recessive and lethal genetic disorder caused by mutations in the *FLVRC2* gene in humans (9). However, the natural history, pathological progression, and mechanisms driving the phenotype in this disease are unknown. In previous RNA sequencing studies, we and others found *Flvcr2* to be highly expressed at the BBB in mice relative to other organ vasculature [**Fig. S1** and (3, 15)]. To confirm this, we generated tools to study the expression pattern of the gene and its function *in vivo*. To assess the expression of the *Flvcr2* locus we generated an *Flvcr2* conditional knock-in/knock-out eGFP reporter mouse (hereafter termed *Flvcr2*^{GFP}; **Fig. S1A**). In this mouse line, the *Flvcr2* locus was mutated by targeted recombination to insert loxP sites flanking the second exon of the *Flvcr2* gene and an inverted GFP cassette, which is also flanked by mutated loxP sites. Upon Cre-mediated recombination, the GFP cassette is irreversibly flipped in-frame, while the second exon is removed, leading to the inactivation of the gene and the expression of GFP under the control of the endogenous locus. To generate a knockout (null) allele, we crossed the floxed line with mice carrying a Cre transgene expressed under the control of the *Mef2c* promoter, which recombined the floxed allele in the germline.

We found that *Flvcr2* mRNA (as assessed by the GFP reporter) is most highly expressed in the brain compared to other major organs in adult mice (**Fig. S2**). We also detected GFP reporter expression in presumed alveolar macrophages in the lung, and sparse signal in intestinal epithelial cells and hepatocytes (**Fig. S2**). Consistent with published bulk and single cell expression datasets (**Fig. S3A**) (16), we observed GFP expression in all vascular segments (i.e. arteries, veins, and capillaries) in a pattern consistent with endothelial

cells in adult animals (**Fig. S3B**), as well as in embryos (**Fig. S3C**). Since *Flvcr2* expression is detected also in pericytes in single-cell transcriptomic dataset, albeit at lower level and/or in a smaller subset of the cells (16), it is possible that some of the GFP signal emanates from pericytes, however, this would be hard to unequivocally establish given the stronger or more prevalent expression in the neighboring endothelial cells.

PVHH is a distinctly developmental disorder, affecting mid-late gestation fetuses. We used our *Flvcr2*^{GFP} reporter line to track expression during embryonic development. We first detected GFP in a subset of brain endothelial cells around embryonic day (E)12.5 (**Fig. 1A**, arrow). Subsequently, both the number and proportion of GFP-expressing brain endothelial cells increased until E18.5, at which time most CNS endothelium was GFP-positive (**Fig. 1B**). We also detected GFP signal in the syncytiotrophoblasts of the placenta and yolk sac visceral endoderm (**Fig. S3C**), but not in any other tissues in the embryo proper. Finally, flow cytometry analysis of cells from whole E14.5 brains (**Fig. S4A**) confirmed that the vast majority of the GFP+ cells were also CD31 positive, however about 10% of these were GFP negative, potentially corresponding to *Flvcr2* positive pericytes. Embryonic blood cells from *Flvcr2*^{GFP} mice did not express GFP (not shown).

Reduced brain vascularization in *Flvcr2* mutant mice.

To investigate the function of *Flvcr2* in mice, we generated mice knockouts by intercrossing heterozygous *Flvcr2*$^{+/GFP}$. *Flvcr2*$^{+/GFP}$ mice were born at mendelian frequencies, and were healthy and fertile; however, we failed to recover nullizygous *Flvcr2*$^{GFP/GFP}$ mice at weaning age, demonstrating that *Flvcr2* gene inactivation causes embryonic or early postnatal lethality (**Table 1**). Newborn *Flvcr2*$^{GFP/GFP}$ pups could only survive for a few hours after birth with signs

of severe hypoxia (cyanosis, reduced movement). We did not observe any gross malformation in mutant embryos.

We next focused on brain vascular phenotypes in mutant embryos. Flow cytometry analysis of brain endothelial cells from embryos at E15.5 confirmed increased GFP signal in *Flvcr2*$^{GFP/GFP}$ samples compared to *Flvcr2*$^{+/GFP}$ endothelium (**Fig. S4D**). Coronal sections through *Flvcr2*$^{+/GFP}$ and *Flvcr2*$^{GFP/GFP}$ brains revealed striking vascular malformations in the median and lateral ganglionic eminences (GE) (**Fig. 1A,B**). Time course analyses indicate that periventricular vessels in *Flvcr2*$^{GFP/GFP}$ embryos were apparently normal at E12.5 (an early stage of vascular growth in the brain), but became progressively hypoplastic from E14.5 until E18.5. Vascular malformations led to a reduction in the area of the brain periventricular parenchyma covered by vessels (**Fig. 1C**) and dilation of vascular tubes with "clumping" of ERG+ endothelial nuclei within vessel walls (**Fig. 1B,D**). Furthermore, these vessels appeared to stall in their ingression toward the ventricular zone forming a vascular plexus ~300um from the ventricles compared to the periventricular plexus (PVP) which normally forms immediately adjacent to the ventricular surface (**Fig. 1E**). The localization of vascular anomalies to the periventricular vascular plexus suggests that vessels in this region are particularly sensitive to *Flvcr2* gene disruption. The vascular phenotype and embryonic lethality was recapitulated in mice with endothelial cell-specific deletion of *Flvcr2*, generated by crossing floxed mice with animals carrying a Cre recombinase transgene under the control of the *Tek* promoter (*Flvcr2*$^{fl/fl}$*;Tek-Cre*, referred to as *Flvcr2*$^{\Delta EC}$) (**Fig. 1F; Table 2**), confirming that *Flvcr2* largely functions in brain endothelial cells, as would be predicted based on the Flvcr2 expression pattern. Of note, we observed enlarged ventricles in *Flvcr2*$^{GFP/GFP}$ embryos at E18.5 (**Fig. 1G,H**), reminiscent of the hydrocephalus phenotype observed in humans with PVHH.

Reduced vascular growth in brains lacking *Flvcr2* leads to hypoxia and cell death.

We next sought to evaluate the pathological consequences of impaired vascularization in the GE. We hypothesized that impaired angiogenesis and reduced cerebral vascularization in *Flvcr2*$^{GFP/GFP}$ mutants might lead to hypoperfusion of the brain, and subsequent hypoxia and tissue infarction. Consistent with this model, we observed a strong signal of pimonidazole (hypoxyprobe) adducts in GE regions devoid of blood vessels in *Flvcr2*$^{GFP/GFP}$ embryos at E14.5 and E18.5 (**Fig. 2A,B**), indicating the presence of low oxygen tension in these avascular tissues. Hypoxia normally induces angiogenesis largely through the activation of HIF-1α translocation to the nucleus, promoting its activity as a transcription factor, and leading to the expression of VEGF (17). We observed increased HIF-1α nuclear staining specifically in the progenitor population located in the avascular GE of *Flvcr2*$^{GFP/GFP}$ embryos (**Fig. 2C**), concomitant with a striking increase in VEGF-A immunoreactivity in the same area, compared to the well vascularized GE of *Flvcr2*$^{+/GFP}$ control embryos (**Fig. 2D**). Unabated hypoxia from reduced vascularization causes metabolic collapse, tissue infarction, and cell death. Using active caspase 3 immunostaining, we observed massive cell death in the ventral parts of the brain of *Flvcr2*$^{GFP/GFP}$ embryos at E18.5 (**Fig. 2E**), concentrated in areas lacking blood vessels. Interestingly, there were relatively few apoptotic endothelial cells in the brain, and there was little apoptosis observed at early time points (E14.5) even in the presence of vascular malformation and tissue hypoxia. These observations suggest that endothelial cell apoptosis is an unlikely mechanism underlying vascular malformation and downstream sequelae in *Flvcr2*$^{GFP/GFP}$ mice. Together, these data support our model that impaired vascular growth in brains of *Flvcr2*$^{GFP/GFP}$ embryos leads to hypoxia and tissue infarction, providing a possible explanation for the ultimate death of the mutant animals.

After tissue ischemia/infarction in the brain and other organs (e.g. heart), monocytes/macrophages rapidly accumulate within the damaged tissue, leading to the production of inflammatory mediators (18, 19). These cells can directly affect vascular morphogenesis and neurovascular integrity (20, 21). Indeed, we observed a temporal trend in *Flvcr2*$^{GFP/GFP}$ embryos to accumulate myeloid cells in the brain, which was not seen in control embryos (**Fig. S5A,B**). To assess the relevance of increased myeloid cell population in the embryo brain, we depleted them by pharmacological inhibition of CSF1R with PLX5622 in one litter (22). We did not detect any IBA1^{+} PU.1^{+} cells in the embryos from this litter at E18.5 (**Fig. S5C**), indicating successful depletion of the myeloid lineage. However, the phenotypic consequences of *Flvcr2* inactivation were present; we observed severe vascular malformations and massive cell death in the brain of *Flvcr2*$^{GFP/GFP}$ embryos (**Fig. S5D**). This result suggests that increased infiltration of macrophages does not drive the alterations found in *Flvcr2*$^{GFP/GFP}$ embryos.

***Flvcr2* inactivation impairs angiogenic sprouting.**

Within the periventricular vascular plexus, vascular growth is predominantly mediated by sprouting angiogenesis (23, 24), wherein endothelial cells of the vascular front (tip cells) extend filopodia into avascular regions toward the cerebral ventricles and initiate anastomosis with neighboring tip cells. This process is driven by tissue-derived VEGF gradients which signal through endothelial VEGFR2 (encoded by the *Kdr* gene), and further regulated by various other pathways that can influence VEGF signaling such as DLL4-NOTCH, NRP1, and WNT, among others (25, 26).

To understand the molecular alterations in endothelial cells associated with *Flvcr2* inactivation, we sought to define their transcriptional landscape in *Flvcr2*$^{GFP/GFP}$ embryos.

Using fluorescence activated cell sorting, we isolated GFP+ CD31+ cells from embryonic brains at E15.5 and defined their transcriptional profile by RNA-Seq. Within this transcriptomic data, we detected differential expression in 28 genes involved in sprouting angiogenesis in *Flvcr2*$^{GFP/GFP}$ mutants compared to *Flvcr2*$^{+/GFP}$ controls (~25% of genes associated with sprouting angiogenesis in the Gene Ontology database; **Fig. 3A** and **Table 3**), suggesting a regulatory role for *Flvcr2* in the brain angiogenic program. Interestingly, by re-analyzing single-cell transcriptomic data from chronically hypoxic brain (27), we found some of these genes were upregulated in a hypoxia-specific population of endothelial cells (**Fig. 3B**), including *Dll4*, *Esm1*, and *Flt4* (which codes for VEGFR3). This suggests that hypoxia may drive the transcriptional response observed in *Flvcr2*$^{GFP/GFP}$ endothelial cells. Next we evaluated the protein levels of these genes by western blot and/or immunofluorescence (**Fig. 3C-E**). For the total protein analyses by western blot, we isolated vascular fragments from E15.5 brains to enrich for endothelial cells and reduce possible signals from neural progenitors. At the whole-brain vasculature level, we observed an increased in the protein levels of DLL4 and VEGFR3 (**Fig. 3B**). We next assessed if these proteins were increased specifically in the LGE using immunofluorescence. As expected, DLL4 and ESM1 were localized in the more tip-like cells of the LGE periventricular plexus in control *Flvcr2*$^{+/GFP}$ embryos (**Fig. 3C**), in sharp contrast to mutant embryos, in which these proteins localized to endothelial cells of the malformed vessels, deeper into the LGE (**Fig. 3C**). In addition, the fluorescence intensity of VEGFR3 and ESM1 was increased in the endothelial cells of the LGE from *Flvcr2*$^{GFP/GFP}$ embryos, compared to *Flvcr2*$^{+/GFP}$ controls (**Fig. 3D**).

Mice with inactivation of WNT/β-Catenin signaling or TGF-β signaling have brain vascular phenotypes and ventriculomegaly similar to that observed in *Flvcr2* mutants (7, 8, 28). To assess whether these pathways were affected in *Flvcr2* mutants, we performed

western blots (from brain vascular fragments) and immunohistochemistry probing for downstream targets in these pathways. These experiments indicated that phosphorylated SMAD3 (a canonical TGF-β signaling target) was unchanged in endothelial cells from *Flvcr2* mutants (**Fig. S6A,B**). Similarly, based on western blot for AXIN2 (a direct target of WNT/β-catenin signaling, (29)) and using a WNT/β-Catenin reporter mouse (28) crossed to inducible endothelial cell specific *Flvcr2* mutants or controls, we observed no evidence of repression (or activation) of WNT-signaling (**Fig. S6C,D**). Finally, we took a genome-wide approach and compared the transcriptional profiles of endothelial cells lacking *Flvcr2*, *Tgfbr2*, or *Ctnnb1* (**Fig. S6E**). To inactivate *Tgfbr2* in endothelial cells, we produced *Tgfbr2*$^{fl/fl}$; *R26*^{TdTomato}; *Cdh5-CreER* embryos from dams injected with tamoxifen on days E11, E12, and E13. We sorted endothelial cells from these mice based on the expression of TdTomato and performed RNA-Seq in the same manner as with *Flvcr2*$^{GFP/GFP}$ endothelial cells. The transcriptional profile from *Ctnnb1* deficient cells was obtained from the literature (3); in that study, authors performed TRAP-Seq of brain endothelial cells at E14.5. By intersecting these three datasets, we observed only limited similarity between *Flvcr2*$^{GFP/GFP}$ endothelial cells and the other two types of mutant endothelium (**Fig S6E**).

Together, these data suggest that endothelial cells from *Flvcr2*$^{GFP/GFP}$ embryos maintain high levels of some elements of the response machinery to enforce angiogenic cues; however, the reduction in vessel ingression into the GE in the presence of high levels of VEGF suggests the mutant endothelial cells are unable to transduce those signals, independently of alterations in TGF-β or WNT/β-catenin signaling pathways.

Normally, tissue-derived VEGF gradients in growing or hypoxic tissue drive sprouting angiogenesis primarily through two distinct but related cellular processes: tip/stalk cell selection and endothelial proliferation (30). Endothelial cells at the angiogenic front are

exposed to high levels of VEGF which signal through VEGFR2, enforcing an endothelial tip cell phenotype with numerous and elaborate filopodia. Further from the angiogenic front endothelial cells are exposed to lower levels of VEGF and adopt stalk positions (31). During angiogenic growth, individual endothelial cells actively swap into tip and stalk cell positions (30), and simultaneously proliferate to generate more cells supporting the growing vascular structures. We were surprised to find that brain blood vessels in *Flvcr2* mutants failed to grow even in the presence of supra-physiologic VEGF levels, and therefore sought to determine what aspect of sprouting angiogenesis might be affected in these mutants.

First, to identify proliferating endothelial cells in the embryo brain, we used KI67 and ERG immunostaining, which mark nuclei from cycling and endothelial cells, respectively (**Fig. 4A**). We detected a reduction in KI67+ endothelial cells at E14.5 in the GE of *Flvcr2*$^{GFP/GFP}$, and we observed no change in proliferating endothelial cells at E12.5 (**Fig. 4B**). However, the number of endothelial cells per vessel length was unchanged at both embryonic stages (**Fig. 4C**). Since endothelial cells in the GE are exposed to high levels of VEGF at E14.5, these results support an impaired proliferative response to angiogenic cues in endothelial cells lacking *Flvcr2*.

Next, we considered whether tip/stalk cell selection could be affected by loss of *Flvcr2*. Consistent with an overall impaired endothelial response to angiogenic signals, we observed a strong reduction in the number (**Fig. 4D,E**) and length (**Fig. 4F**) of filopodia produced by mutant *Flvcr2*$^{GFP/GFP}$ versus control *Flvcr2*$^{+/GFP}$ endothelial cells at the vascular front, both at E12.5 (prior to other vascular abnormalities) and E14.5.

The observed reduction in filopodia could be due to abnormal specification of endothelial cells in the correct position and/or the failure of endothelial cells to sort to appropriate tip and stalk positions within a vascular segment. To differentiate these

possibilities, we generated *Flvcr2* endothelial mosaics with sparse tamoxifen-inducible recombination in the *Flvcr2* locus using *Cdh5-CreERT2* (*Flvcr2*$^{\Delta iEC}$). We crossed *Flvcr2*$^{+/fl}$;*Cre*$^{+}$ females with *Flvcr2*$^{fl/fl}$ males to obtain *Flvcr2*$^{fl/fl}$;*Cre*$^{+}$ (*Flvcr2*$^{\Delta iEC/\Delta iEC}$; mutants) and *Flvcr2*$^{+/fl}$;*Cre*$^{+}$ (*Flvcr2*$^{+/\Delta iEC}$; controls) embryos within the same dam. Pregnant mice were injected with three doses of tamoxifen (2 mg per dose per animal) on consecutive days (E10.5, E11.5, E12.5). Since, both mutant and control embryos carry the targeted allele, we took advantage of endogenous GFP reporter expression to identify mutant endothelial recombinants among non-recombined wild-type cells in the lateral GE at E14.5. An important caveat to this approach is the possibility that some cells in *Flvcr2*$^{\Delta iEC/\Delta iEC}$ embryos may have only one recombined allele (i.e. heterozygous for *Flvcr2*^{GFP}). Thus, our analyses may underestimate any phenotype associated with *Flvcr2* inactivation. We defined “tip-like” positions as those within the first 50 μm from the ventricle (**Fig. 4G**), based on the localization of the periventricular plexus, the greater number of filipodia per vessel length in this area (7), and the expression of prototypical markers such as ESM1 (**Fig. 1D**, **Fig. 3B**). We defined “stalk-like” positions as those outside of the tip-like position (**Fig. 4G**). In *Flvcr2*$^{+/\Delta iEC}$ embryos, the distribution of recombined cells was not different between the tip-like and stalk-like positions, as expected from unhampered sorting of recombined cells (**Fig. 4H,I**). However, in *Flvcr2*$^{\Delta iEC/\Delta iEC}$ embryos, recombined cells localized mainly to the stalk-like position (**Fig. 4H,I**). Taken together, these experiments indicate that endothelial cells lacking *Flvcr2* are intrinsically impaired in their angiogenic capacity, likely due to a reduced ability to adopt a tip cell phenotype and an apparent inability to proliferate in response to supra-physiologic levels of VEGF. In the mosaic recombination setting, wild-type cells appear to compensate for *Flvcr2* mutant endothelium which tend not to reach the tip position, allowing for relatively normal vascular network formation, with only a few exceptions (as illustrated in **Fig. S7**).

VEGFR2, the most important VEGF receptor in endothelial cells, promotes tip cell selection and endothelial proliferation (31). Furthermore, brain endothelial cell specific deletion of VEGFR2 and antibody mediated blockade of VEGFR2 in mouse embryos cause a similar vascular phenotype as we observed in *Flvcr2* mutants (32, 33). Based on this, we looked to determine how *Kdr*/VEGFR2 may be regulated in *Flvcr2* mutant mice. We found *Kdr* mRNA levels comparable to control in our RNA-Seq from isolated brain endothelial cells. However, there was a striking reduction in the protein levels of VEGFR2 in western blots from isolated brain vascular fragments suggesting that expression of VEGFR2 is post-transcriptionally down-regulated in mice lacking *Flvcr2* (**Fig. 4J,K**). Downregulation of VEGFR2 could be a primary consequence of reduced *Flvcr2*, or secondary to its increased downregulation following hypoxia-driven expression of VEGF (34). Taken together, these results indicate that *Flvcr2* expression is required for sprouting angiogenesis in the brain, and that the vascular abnormalities observed in $Flvcr2^{GFP/GFP}$ mutants may be a consequence of reduced VEGFR2-mediated endothelial cell sprouting.

***Flvcr2* is dispensable for establishing and maintaining the blood-brain barrier.**

Brain angiogenesis is very tightly coupled to the formation of the BBB, and other mutant mice with vascular phenotypes similar to $Flvcr2^{GFP/GFP}$ embryos (e.g. WNT/β-catenin pathway mutants (8), TGF-β pathway mutants (7)), also have defective BBB. Here, we tested BBB formation and maintenance in *Flvcr2* mutant mice using markers of hemorrhage (extraluminal red blood cells) and various tracers of vascular leakage (**Fig. 5A**). We used previously published $Tgfbr2^{fl/fl};Cdh5\text{-}Cre^{ERT2}$ embryos ($Tgfbr2^{\Delta iEC/\Delta iEC}$), known to develop BBB defects and severe brain hemorrhage by E14.5 (7) as positive controls (**Fig. 5A**). To our surprise, we found no evidence of hemorrhage or vascular leakage (perfused dextran-TMR

10 kDa, endogenous IgG) in the brains of *Flvcr2*-deficient embryos at any analyzed stage, even in areas with severe vascular malformations or tissue infarction (**Fig. 5A-C**). Consistent with these results, immunostaining for canonical markers of BBB junctional protein CLDN5 (enriched in endothelia with an mature BBB) and PLVAP (enriched in fenestrated endothelia) in embryos revealed no change in these proteins in *Flvcr2*$^{GFP/GFP}$ mutants compared to controls (**Fig. S8A**). Furthermore, we observed no evidence of BBB dysfunction in adult *Flvcr2*$^{\Delta iEC/\Delta iEC}$ mutants, using several different vascular tracers including sulfo-NHS-biotin, Cadaverin-555, and evans blue (**Fig. 5D-G**). Of note, dextran-TMR 10 kDa and sulfo-NHS-biotin tracers were observed inside vascular lumens of perfused mice, confirming adequate distribution of the tracer, as well as vascular lumenalization and perfusion of vessels in both *Flvcr2*$^{GFP/GFP}$ embryos and adult *Flvcr2*$^{\Delta iEC/\Delta iEC}$ mice (**Fig. 5**). In adult *Flvcr2*$^{\Delta iEC/\Delta iEC}$ mice there was no histological evidence of brain hemorrhage in any *Flvcr2* mutant, and no major vascular abnormalities or other obvious phenotypic changes. It is worth noting that, with the tamoxifen regime used here, the possibility remains that some endothelial cells in *Flvcr2*$^{\Delta iEC/\Delta iEC}$ still possess one intact allele, making them heterozygous. In order attempt to address this issue we took two distinct approaches. First, we induced gene inactivation at early postnatal days (P1, P2, and P3), a time point that other endothelial-specific tamoxifen-inducible mouse models have dysfunctional BBB (e.g. GPR124 mutants (28)) and analyzed the BBB using the biotin tracer at P15. In this setting, we detect strong GFP signal in brain vessels, but we did not observe evident extravasation of the biotin tracer (**Fig. S8B**). Second, we crossed *Flvcr2*$^{fl/fl}$*;Cdh5-CreER* mice with *Flvcr2*$^{+/GFP}$ to obtain animals with one floxed allele and one null allele in the presence of the tamoxifen-dependent Cre recombinase (*Flvcr2*$^{\Delta iEC/GFP}$). With this strategy, only one allele must be recombined to produce a mutant cell; however, the presence of the null allele in all cells precludes our ability to track recombination of the *Flvcr2*

locus, since all cells expressing *Flvcr2* will be GFP+. We induced recombination with 4 doses of tamoxifen and evaluated biotin leakage 20 days later. Again, we failed to observe leakage above control levels in the brain parenchyma (**Fig. S8C**).

Reduced pericyte coverage is associated with BBB defects (35), and a previous study documents reduced vascular mural cell staining in brain autopsy specimens from patients with Fowler Syndrome (36). We observed normal pericyte coverage (area of CD31 vessels covered by NG2+ pericytes) at E12.5 and E14.5, and a slight reduction at E18.5, in *Flvcr2*$^{GFP/GFP}$ mutant embryos (**Fig. S8D**), suggesting that pericyte abnormalities are a mild, late, and likely a downstream event in PVHH pathogenesis, and that these abnormalities are insufficient to affect BBB properties in *Flvcr2* mutant mice. Taken together, these data indicate that *Flvcr2* is dispensable for the establishment and maintenance of the BBB in mice, and is apparently dispensable for the maintenance of vascular morphology/structure in adult mice.

DISCUSSION

Here, we report on the creation of a mouse model of PVHH that recapitulates the features of the human syndrome. We describe the associated vascular malformations, their consequences, and provide evidence supporting a mechanism for their development, involving impaired vascular sprouting due to reduced responsiveness to angiogenic cues. Interestingly, we observed a functional BBB in the mutants, using a comprehensive array of tracers.

Several mouse mutants have been described to present brain vascular malformations during embryonic development. These mutants disrupt distinct signaling pathways, including TGF-β/Integrin β-8 (7, 37), Neuropilin-1 (38), and WNT/β-Catenin (8, 28). Some of these pathways may interact through unknown mechanisms to drive brain angiogenesis, since their individual disruptions lead to severe, yet very similar, phenotypes. Of special note, these mutants share widespread CNS vascular malformations, affecting all parts of the brain and the spinal cord even at early-mid stages (E14.5). Furthermore, they show massive hemorrhage in the brain parenchyma and/or disruption of the BBB, depending on timing and degree of gene deletion (28). It is interesting that mouse mutants with isolated disruption of the BBB -without vascular malformations- do not present with extravasation of red blood cells (4–6). This has led to the conceptualization that vascular morphogenesis and stabilization are coupled; thus, blood vessel malformation and destabilization invariably lead to the spilling of luminal contents including tracers and blood. Further support for this concept comes from pathological conditions, such as cerebral cavernous malformation (CCM), which is associated with intracerebral bleeding in mice and humans (39). In the studies presented here, we challenge this view by demonstrating the presence of severe vascular malformations in the brain, without evidence of destabilization. We failed to find hemorrhage in the brains of

Flvcr2$^{GFP/GFP}$ embryos, and we provide compelling evidence for a functional BBB in these mutants. Importantly, this indicates that downstream pathological consequences in *Flvcr2*$^{GFP/GFP}$ mice (hypoxia, tissue infarction, death) stem from impaired vascularization of the brain, and not from secondary damage due to hemorrhage or vascular leak. We anticipate that this model, in combination with those mentioned above, will permit the study of brain angiogenesis in separation from BBB maturation. This work may lead to potential therapeutic targets for the treatment of vascular disorders in the brain.

Humans with mutations in the *FLVCR2* gene develop PVHH, with a phenotype similar to that observed in *Flvcr2*$^{GFP/GFP}$ embryos; however, disease presentation varies in timing, severity, and accompanying symptoms. Pathognomonic features of PVHH include hydrocephalus and vascular abnormalities ("glomeruloid vascular proliferation") involving parenchymal blood vessels in various regions of the brain. Associated brain calcification and necrosis in the white matter, basal ganglia, brainstem, cerebellum, and spinal cord; other central nervous system malformations (e.g. hypoplastic cerebellum); retinal vascular abnormalities; and extra-neural manifestations (ranging from intrauterine growth restriction to severe arthrogryposis with fetal akinesia sequence) are more variably present. While early descriptions and prenatal ultrasound provided evidence of hydranencephaly (absent cerebral hemispheres), post-mortem examinations have more typically revealed a hemispheric mantle, indicating moderate to severe hydrocephalus. Based on histological examination of post-mortem tissues, the vascular lesions are generally described as "glomeruloid" due to superficial resemblance to renal glomeruli. We believe that the term "proliferation" has been used descriptively; to our knowledge there is no direct evidence of vascular cellular proliferation in PVHH lesions. With the exception of two reported cases of PVHH born alive, the disease causes mid- to late-gestation fetal demise. Compared to these descriptions of

PVHH in humans, our mouse models with *Flvcr2* gene deletion consistently reproduce the most common features of human PVHH including severe brain vascular malformation, ventriculomegaly/hydrocephalus, and fetal or early post-natal demise. We do not find evidence of the more variable symptoms present in humans such as fetal akinesia, and do not find evidence for vascular proliferation.

In human specimens, it has been impossible to determine the cause of the pathological findings, since there is no access to the time course of the disorder. However, some authors had speculated that the primary problem was that of the vasculature (36). Similar to humans with PVHH (12), we observed hydrocephalus/ventriculomegaly in *Flvcr2*$^{GFP/GFP}$ embryos, but without destruction of the cortex. We suspect that enlarged ventricles are a consequence of reduced tissue growth (hydrocephalus *ex vacuo*) stemming from abnormal vascularization, tissue hypoxia, and cell death. We show that endothelial cell-specific deletion of *Flvcr2* leads to a primary impairment in brain vascular sprouting. We propose that the disease is initiated in the more proliferative parts of the brain, which expand rapidly; therefore, vessels need to grow at a faster pace to provide appropriate oxygenation. A similar scenario has been proposed for the brain vascular malformations caused by neonatally induced endothelial-specific knockout of the small GTPase *Cdc42*; the resulting malformations affect mostly the cerebellum and the retina, i.e. parts of CNS that grow rapidly in the neonatal period (40).

The constitutive *Flvcr2* inactivation studied here caused reduced brain vessel growth already in the embryo, leading to impaired perfusion of the rapidly growing germinal matrix, resulting in hypoxia and a subsequent massive increase in VEGF production. In fact, some or all of the gene expression changes present in *Flvcr2* mutant endothelial cells at E14.5 may be a consequence of hypoxia. Comparing our transcriptomic data to single endothelial cell transciptomes from hypoxic brains revealed remarkable similarity. It is important to note that

many of the genes common to both angiogenesis and hypoxia, are in fact *negative* regulators of angiogenic sprouting and proliferation (e.g. DLL4 and high VEGF). Therefore, changes to these genes might not merely reflect the presence of brain hypoxia, but may actually drive the vascular response to it. For example, over-expression of VEGF in the developing mouse brain induces the formation of vascular abnormalities that are similar to those observed in *Flvcr2* mutant mice (41). Paradoxically, brain endothelial specific deletion of *Vegfr2* or blocking VEGFR2 with antibodies during early brain development also promotes the formation of similar ("glomeruloid") brain vascular abnormalities (32, 33), suggesting that VEGFR2 downregulation in the setting of high VEGF might lead to these vascular phenotypes. A similar phenomenon is observed in the retina where high mitogenic stimulation by VEGF arrests the proliferation of angiogenic vessels (42). Therefore, it is possible that hypoxia-induced VEGF overproduction has the counter-intuitive effect of potentiating the anti-angiogenic effects of *Flvcr2* disruption, exacerbating vascular malformation. VEGF overproduction might also be the cause of the reduction of VEGFR2 that we observe in *Flvcr2* mutants, similar to what has been described in other studies (34).

If tissue hypoxia and resulting angiogenic abnormalities are part of the Fowler syndrome pathogenesis, then what are the primary effects of *Flvcr2* knockout that cause tissue hypoxia? To address this, we first focused on changes in blood vessels that occur prior to the onset of hypoxia. We found that periventricular endothelial cells had a marked reduction in filopodia number and length at E12.5, suggesting a primary problem with angiogenic sprouting in the brain, and in particular the tip cells. This abnormality preceded all other observable changes. We then took advantage of the variable degrees of endothelial recombination in tamoxifen-inducible mutants to study this process in more detail. Importantly, in endothelial mosaics with low proportions of mutant/recombined endothelial cells, there was

no evidence of hypoxia or glomeruloid vascular malformation. In these animals we found that *Flvcr2*$^{+/GFP}$ (heterozygous) endothelial cells distributed randomly throughout the brain vasculature, with equal contribution to tip and stalk positions), whereas *Flvcr2*$^{GFP/GFP}$ (presumed to be homozygous knockout) mutant endothelial cells were found predominantly in the stalk position, and less often in the tip position near the brain ventricle. We presume this is because wild type endothelial cells compensate for mutant endothelial cells by preferentially taking the tip/sprouting position, allowing for normal vascular growth. As would be predicted, in individual *Flvcr2* mutants with a high burden of recombination (the most extreme example being the conventional null), there are inadequate numbers of wild type endothelial cells to compensate for the presence of mutant endothelial cells, resulting in a more fulminant phenotype. Also, this scenario is analogous to what has been proposed for endothelial-specific *Cdc42* knockout, which leads to an inability of the tip cells to form filopodia and migrate to populate the peripheral parts of the developing retina. In mosaic situations where *Cdc42*-negative endothelial cells are in minority, those cells arrest and become overtaken by wild-type tip cells, resulting in the formation of an essentially normal vessel network. Only when *Cdc42*-negative endothelial cells are in majority and hence forced to occupy tip positions, angiogenic sprouting gets impaired (40, 43).

Together these results demonstrate an integral, cell-autonomous requirement for *Flvcr2* in brain tip cell selection and angiogenic sprouting. Failure of angiogenic sprouting leads to subsequent hypoxia, with resultant activation of an angiogenic program (e.g. DLL4 and VEGFR3) that further exacerbates the vascular pathology when sprouting is deficient. Future studies utilizing single cell transcriptomics in mosaic mutants should help to further resolve primary from secondary vascular responses to *Flvcr2* mutation.

The molecular function of the FLVCR2 protein is controversial. A study suggests that it acts as a heme importer (11), in line with its homology and sequence similarity with FLVCR1, a heme transporter (44). Heme, the prosthetic moiety for numerous heme proteins, serves as a central regulator of oxygen transport (hemoglobin), aerobic metabolism (electron transport cytochromes), redox sensing, and gene transcription in erythroid and non-erythroid cells (45). Although the heme transport function of FLVCR2 has not yet been tested in endothelium, we speculate that reduced endothelial cell heme due to mutation or knockout of *Flvcr2* might directly affect metabolic pathways involving heme, and/or dys-regulate transcriptional programs normally modulated by heme-binding transcription factors such as NR1D1/2 (RevERBα/β) or BACH1 (46, 47). Of note, these transcription factors have been shown to regulate different aspects of angiogenesis (48, 49). An important next step will be to determine directly whether these heme pathways are affected by *Flvcr2* mutation, and the effects of endothelial heme on vascular sprouting.

In conclusion, we have developed a new mouse model of the rare disease PVHH, which provides important insights into the regulation of brain angiogenesis by disentangling morphogenesis of this vascular bed from vessel stabilization.

METHODS

Generation of the floxed *Flvcr2* allele. Mice with a *Flvcr2* FLEx (*Flvcr2*^{GFP}) allele were generated by Biocytogen (Beijing, China). Briefly, the targeting vector was constructed as shown in **Fig. S1A**, linearized, and transfected into C57BL/6J embryonic stem (ES) cells (Beijing Biocytogen Co., Ltd, China) by electroporation. G418-resistant ES clones were screened for homologous recombination by PCR. Correctly targeted clones were confirmed by Southern blot analysis and sequencing. Two positive clones were injected into Balb/c blastocysts and implanted into pseudopregnant females to generate chimeric mice. Chimeric mice were bred to C57BL/6J mice to obtain F1 mice carrying the recombined allele containing the FLEx construct.

Animals. Animals carrying the *Flvcr2*^{GFP} allele were maintained on a C57Bl6 background in specific pathogen-free conditions at University of California, San Francisco, CA, USA. All animals had access to food and water *ad libitum*. *Flvcr2*$^{+/GFP}$ animals were generated by crossing to *Mef2c-Cre* mice (kind gift from Dr. Brian Black at Cardiovascular Research Institute, UCSF, San Francisco, CA). *Tek-Cre* (Tg(Tek-cre)5326Sato) and *Cdh5-CreER*^{T2} (Tg(Cdh5-cre/ERT2)1Rha; kind gift from Dr. Ralf Adams at Max Planck Institute for Molecular Biomedicine, Muenster, Germany) were used for endothelial cell recombination. Mice carrying the *R26-TCF/LEF-LSL-H2B-GFP* allele (Gt(ROSA)26Sor$^{tm12(Tcf/Lef-GFP*)Nat}$) were a kind gift from Dr. Jeremy Nathans at John Hopkins University (Baltimore, MD). *Tgfbr2*$^{fl/fl}$ (Tgfbr2^{tm1Karl}) mice have been reported previously (50). The *Ai14* allele (Gt(ROSA)26Sor$^{tm14(CAG-tdTomato)Hze}$/J) was obtained from Jackson Labs (Bar Harbor, ME). DNA extracted from the mouse tails was analysed by polymerase chain reaction (PCR) for genotyping using primers in **Table S1** or as recommended by Jackson Labs.

Embryo collection. For all crosses, one 2-6 month old male was house with two 2-4 month old females and the presence of vaginal plugs was assessed every morning. Pregnant females were euthanized at the appropriate embryonic age (E12.5, E14.5, E15.5, or E18.5) by CO_2 asphyxiation or isofluorane saturation, and cervical dislocation. Some dams were injected i.p. with 180 mg pimonidazole 3 hours before euthanasia. Uteri were retrieved from the abdominal cavity and individual implantation sites were collected. Embryos were separated from the yolk sac and placenta, and the tail tip was saved for genotyping. Tissues were directly dropped in PFA 4% for fixation, flash-frozen, or further processed for vascular fragments separation.

Tamoxifen regimen. To induce cell-specific inactivation of the *Flvcr2* gene, adult mice were injected i.p. three times over 5 days with 2 mg tamoxifen in corn oil. Alternatively, mice were injected three times on consecutive days on P60 and one more on P70 with 2 mg tamoxifen. For juvenile inactivation, pups were injected intra-gastrically on P1, P2, and P3 with 0.2 mg tamoxifen. To produce embryonic mosaic recombination, pregnant dams were injected 2 mg tamoxifen i.p. on days E10.5, E11.5, and E12.5.

Immunofluorescence. Embryonic tissues were fixed overnight in PFA 4%, washed three times in PBS, and frozen in OCT to obtain 20 µm sections in a cryostat. To obtain adult tissues for histological analyses, mice were perfused transcardially with PBS and then with PFA 4%. Tissues were harvested and subsequently processed as embryonic tissue. Sections mounted onto glass were blocked and permeabilized for 2 hours in PBS containing 0.5% Triton X-100, 1% BSA, and 5% normal donkey serum (Sigma, MO) (Blocking buffer). Next, sections were incubated overnight with primary antibodies diluted in Blocking buffer in a humidified chamber. After three washes with 0.1% Tween 20 in PBS, sections were incubated with corresponding secondary antibodies in Blocking buffer for 2 hours, washed again three

times with 0.1% Tween 20 in PBS, and mounted with CC/Mount media (Diagnostics Biosystems, CA). Antibodies are described in **Table S2**. Images were taken using a motorized Zeiss 780 upright laser scanning confocal microscope with a 34 detector array with a water immersion Zeiss Plan Apochromat 20X/1.0 D=0.17 Parfocal length 75 mm (Zeiss, Germany). The spectral configuration was set up using the recommended settings from the Zen software (Zeiss, Germany). Raw images were analyzed in ImageJ and final figures were constructed with GIMP and Inkscape.

Single-cell RNA-Seq re-analysis. Fastq files were first pre-processed using scPipe (51) to produce count matrix for each sample and to filter low quality cells. Next, Seurat was used to regress out cell cycle effects, to integrate all samples with the SCTransformation, and to cluster cells with the Louvain algorithm (52). Cells were projected in a low-dimensional space using PHATE and gene expression was imputed with MAGIC (53, 54). Complete R code for these steps is provided in **Supplementary methods**.

Isolation of vascular fragments. Brains from E15.5 embryos were isolated in ice-cold PBS and disrupted lightly by 5 pestle strokes. Fragmented tissue was centrifuged at 1500 g for 20 minutes at 4^{o}C and resuspended 4 volumes of 18% dextran 70 kDa. Vascular fragments were pelleted by centrifugation at 1500 g for 20 minutes at 4^{o}C. Supernatant was further processed in this manner twice and the three pellets were pooled together.

Western blot. Vascular fragments from embryos were lysed in RIPA buffer (25mM Tris pH 7–8, 150 mM NaCl, 0.1% SDS, 0.5% sodium deoxycholate, 1% NP-40) supplemented with protease inhibitor cocktail (Roche). Proteins were resolved in 10% or 8% acrylamide gels in denaturing conditions and transferred to PVDF membranes. Blots were blocked with 5% BSA 0.01% Tween 20 in TBS for 2 hours, probed with primary antibodies (**Table S2**) overnight at 4^{o}C or for 1 hour at room temperature in blocking buffer, washed three times with 0.01%

Tween 20 in TBS, incubated with corresponding secondary antibodies 1 hour at room temperature in blocking buffer, and washed three times as before. Bound antibody was revealed by chemiluminescence and imaged in a Chemidoc (BioRad, CA).

Fluorescence activated cell sorting. Embryos at E15.5 were retrieved as described above. Brains were dissected out in PBS, minced with scissors, and disgregated by mechanical dissociation followed by enzymatic treatment with DNAse (1.5 mg/ml) and collagenase/dispase (3 mg/ml) for 30 minutes at 37ºC. Dissociated cells were filtered through a 40 µm cell strainer to exclude clumps and centrifuged at 1800 rpm for 5 minutes. After one wash in PBS, the new pellet was resuspended in HBSS containing 5% FBS and stained with anti-CD31 conjugated to APC (2 µm/ml) and DAPI 10 pg/ml. Alternatively, cells from *Tgfbr2*$^{fl/fl}$; *Ai14*; *Cdh5-CreER* embryos were sorted based on the endogenous TdTomato fluorescence. Cells were sorted on a FACSAria 3 cell sorter (BD Biosciences, CA) directly onto RLT Plus buffer.

RNA sequencing. Total RNA was extracted from 2000 – 5000 sorted endothelial cells using the Rneasy Plus micro kit (Qiagen, Germany). cDNAs were prepared from 20 ng of total RNA using the SMART-Seq v4 Ultra Low Input RNA Kit (Takara Bio USA, CA) and libraries were constructed from this cDNA with the Nextera XT DNA Library Prep Kit (Illumina, CA). Quality of the libraries was checked by sequencing in a MiniSeq (Illumina, CA) and equimolar amounts of each library were sequenced in a HiSeq 4000 (Illumina, CA) using single-end 50 pb. Grooming of de-multiplexed reads was performed with FASTQ groomer 1.04. Alignment to the mouse genome (mm10) was done using TopHat2 0.7. Transcript abundance estimation and differential expression significance testing were computed with Cufflinks 2.2.1. Heatmaps were constructed with Cluster 3.0 and visualized with TreeView 3.0beta01. Gene enrichment analysis of Gene Ontology biological processes was performed with PANTHER 14.1.

Blood-brain barrier testing. To test the functionality of the BBB in embryos, the liver from E18.5 embryos still attached to the placental circulation was exposed, and 5 µl of 10 kDa dextran at 4 mg/ml was slowly injected into the liver. Dextran was allowed to circulate for approximately 3 minutes, and the embryonic brain was isolated and fixed.

To assess the BBB in adult mice, animals were perfused transcardially with 10 mg of EZ-Link sulfo-NHS-LC-biotin (Thermo Fisher, MA) in PBS, followed by 4% PFA. Brains were collected and processed as described above for other tissues. Alternatively, mice were injected i.p. with 100 µl of 2% Evans blue and euthanized 24 hours later for tissue collection. Lastly, adult mice were injected i.v. with 0.17 mg cadaverine-Alexa555 (Thermo Fisher, MA) in 100 µl of PBS and euthanized 3 hours later. Mice were perfused transcardially with HBSS, and the forebrain and kidneys were lysed in 1% Triton X-100 in PBS. Fluorescence intensity was determined using a fluorometer.

Data deposition. Sequencing datasets have been deposited under GEO accessions GSE129838 and GSE146487. Previously published single cell RNA-Seq data from hypoxic brains can be found under accession GSE125708.

Statistics. The number of biological replicates was not defined using a statistical framework. To reduce bias, image analyses were performed using ImageJ macros where possible. Blinding to the genotype was not feasible at E14.5 and E18.5, since the phenotype is readily evident.

Graphs show scatter dot plots with the mean ± SEM. Deviations of genotype proportion from the expected value was tested using χ^2 test. Statistical significance of differences between means was evaluated by t-test. T-test was performed because we only tested for the effect of genotype and not age. Paired t-test was used when comparing the difference in distribution of cells in mosaic embryos. A P value less than 0.05 was considered significant. All tests were

two-tailed and were performed using core functions in the R statistical environment version 3.6.1.

Study approval. The studies presented here were conducted following the guidelines of the AVMA and were approved by the Institutional Animal Care and Use Committee at UCSF.

AUTHOR CONTRIBUTIONS

NS, CL, EM, GM, and BJ performed experiments and analyzed data. TA, CB, and DS provided resources. TA supervised the study. NS and TA wrote the original draft. All the authors contributed to and approved the final version of the manuscript.

ACKNOWLEDGMENTS

We are indebted to Dr. Stephen Fancy for his help with AXIN2 western blots. We thank UCSF genomics core and UCSF Center for Advanced Technology for their help in the RNA-Seq experiments. We thank the Laboratory for Cell Analysis at UCSF, which is supported by a National Cancer Institute Cancer Center Support Grant (P30CA082103). This work was funded by NIH/NINDS (K08) to T.A. and the Swedish Science Council, the Swedish Cancer Foundation, the Knut and Alice Wallenberg Foundation, and the Leducq Foundation to C. B. N.S. is supported by AHA Postdoctoral fellowship 20POST35120371.

REFERENCES

1. Vasudevan A, Bhide PG. Angiogenesis in the embryonic CNS. *Cell Adh Migr.* 2008;2(3):167–169.

2. Sabbagh MF et al. Transcriptional and epigenomic landscapes of CNS and non-CNS vascular endothelial cells. *Elife.* 2018;7.

3. Hupe M et al. Gene expression profiles of brain endothelial cells during embryonic development at bulk and single-cell levels. *Sci Signal.* 2017;10(487).

4. Ben-Zvi A et al. Mfsd2a is critical for the formation and function of the blood–brain barrier. *Nature.* 2014;509(7501):507–511.

5. Sohet F et al. LSR/angulin-1 is a tricellular tight junction protein involved in blood–brain barrier formation. *J Cell Biol.* 2015;208(6):703–711.

6. Nitta T et al. Size-selective loosening of the blood-brain barrier in claudin-5–deficient mice. *J Cell Biol.* 2003;161(3):653–660.

7. Arnold TD et al. Excessive vascular sprouting underlies cerebral hemorrhage in mice lacking αVβ8-TGFβ signaling in the brain. *Development.* 2014;141(23):4489–4499.

8. Daneman R et al. Wnt/β-catenin signaling is required for CNS, but not non-CNS, angiogenesis. *Proc Natl Acad Sci USA.* 2009;106(2):641–646.

9. Meyer E et al. Mutations in FLVCR2 Are Associated with Proliferative Vasculopathy and Hydranencephaly-Hydrocephaly Syndrome (Fowler Syndrome). *Am J Hum Genet.* 2010;86(3):471–478.

10. Khan AA, Quigley JG. Heme and FLVCR-related transporter families SLC48 and SLC49. *Mol Aspects Med.* 2013;34(2–3):669–682.

11. Duffy SP et al. The Fowler Syndrome-Associated Protein FLVCR2 Is an Importer of Heme. *Mol Cell Biol.* 2010;30(22):5318–5324.

12. Fowler M, Dow R, White TA, Greer CH. Congenital hydrocephalus-hydrencephaly in five siblings, with autopsy studies: a new disease. *Dev Med Child Neurol.* 1972;14(2):173–88.

13. Radio FC et al. Proliferative vasculopathy and hydranencephaly–hydrocephaly syndrome or Fowler syndrome: Report of a family and insight into the disease's mechanism. *Mol Genet Genomic Med.* 2018;6(3):446–451.

14. Thomas S et al. High-throughput sequencing of a 4.1Mb linkage interval reveals FLVCR2 deletions and mutations in lethal cerebral vasculopathy. *Hum Mutat.* 2010;31(10):1134–1141.

15. Tabula Muris Consortium et al. Single-cell transcriptomics of 20 mouse organs creates a Tabula Muris. *Nature.* 2018;562(7727):367–372.

16. Vanlandewijck M et al. A molecular atlas of cell types and zonation in the brain vasculature. *Nature.* 2018;554(7693):475–480.

17. Fan X, Heijnen CJ, van der Kooij MA, Groenendaal F, van Bel F. The role and regulation of hypoxia-inducible factor-1α expression in brain development and neonatal hypoxic–ischemic brain injury. *Brain Res Rev.* 2009;62(1):99–108.

18. Nahrendorf M, Pittet MJ, Swirski FK. Monocytes: Protagonists of infarct inflammation and repair after myocardial infarction. *Circulation.* 2010;121(22):2437–2445.

19. Hoyer FF et al. Tissue-Specific Macrophage Responses to Remote Injury Impact the Outcome of Subsequent Local Immune Challenge. *Immunity.* 2019;51(5):899-914.e7.

20. Fernández-López D et al. Microglial Cells Prevent Hemorrhage in Neonatal Focal Arterial Stroke. *J Neurosci.* 2016;36(10):2881–93.

21. Fantin A et al. Tissue macrophages act as cellular chaperones for vascular anastomosis downstream of VEGF-mediated endothelial tip cell induction. *Blood.* 2010;116(5):829–40.

22. Rosin JM, Vora SR, Kurrasch DM. Depletion of embryonic microglia using the CSF1R inhibitor PLX5622 has adverse sex-specific effects on mice, including accelerated weight gain, hyperactivity and anxiolytic-like behaviour. *Brain Behav Immun.* 2018;73:682–697.

23. Greenberg DA, Jin K. From angiogenesis to neuropathology. *Nature.* 2005;438(7070):954–959.

24. Lee HS, Han J, Bai H-J, Kim K-W. Brain angiogenesis in developmental and pathological processes: regulation, molecular and cellular communication at the neurovascular interface. *FEBS J.* 2009;276(17):4622–4635.

25. Duran CL et al. Molecular Regulation of Sprouting Angiogenesis. In: Pollock D, ed. *Comprehensive Physiology*. Hoboken, NJ, USA: John Wiley & Sons, Inc.; 2017:153–235

26. Ribatti D, Crivellato E. “Sprouting angiogenesis”, a reappraisal. *Dev Biol.* 2012;372(2):157–165.

27. Heng JS et al. Hypoxia tolerance in the Norrin-deficient retina and the chronically hypoxic brain studied at single-cell resolution. *Proc Natl Acad Sci USA.* 2019;116(18):9103–9114.

28. Cho C, Smallwood PM, Nathans J. Reck and Gpr124 Are Essential Receptor Cofactors for Wnt7a/Wnt7b-Specific Signaling in Mammalian CNS Angiogenesis and Blood-Brain Barrier Regulation. *Neuron.* 2017;95(5):1221–1225.

29. Jho E -h. et al. Wnt/β-Catenin/Tcf Signaling Induces the Transcription of Axin2, a Negative Regulator of the Signaling Pathway. *Mol Cell Biol.* 2002;22(4):1172–1183.

30. Chen W et al. The endothelial tip-stalk cell selection and shuffling during angiogenesis. *J Cell Commun Signal.* 2019;13(3):291–301.

31. Gerhardt H et al. VEGF guides angiogenic sprouting utilizing endothelial tip cell filopodia. *J Cell Biol.* 2003;161(6):1163–1177.

32. Pu W et al. Genetic targeting of organ-specifc blood vessels. *Circ Res.* 2018;123(1):86–99.

33. Tan X et al. Vascular Influence on Ventral Telencephalic Progenitors and Neocortical Interneuron Production. *Dev Cell.* 2016;36(6):624–38.

34. Bruns AF et al. Ligand-Stimulated VEGFR2 Signaling is Regulated by Co-Ordinated Trafficking and Proteolysis. *Traffic.* 2010;11(1):161–174.

35. Armulik A et al. Pericytes regulate the blood–brain barrier. *Nature.* 2010;468(7323):557–561.

36. Harper C, Hockey A. Proliferative Vasculopathy and an Hydranencephalic-hydrocephalic Syndrome: a Neuropathological Study of Two Siblings. *Dev Med Child Neurol.* 1983;25(2):232–239.

37. Arnold TD et al. Impaired αVβ8 and TGFβ signaling lead to microglial dysmaturation and neuromotor dysfunction. *J Exp Med.* 2019;216(4):900–915.

38. Gu C et al. Neuropilin-1 conveys semaphorin and VEGF signaling during neural and cardiovascular development. *Dev Cell.* 2003;5(1):45–57.

39. Fischer A, Zalvide J, Faurobert E, Albiges-Rizo C, Tournier-Lasserve E. Cerebral cavernous malformations: from CCM genes to endothelial cell homeostasis. *Trends Mol Med.* 2013;19(5):302–308.

40. Castro M et al. CDC42 Deletion Elicits Cerebral Vascular Malformations via Increased MEKK3-Dependent KLF4 Expression. *Circ Res.* 2019;124(8):1240–1252.

41. Yang D et al. Overexpression of vascular endothelial growth factor in the germinal matrix induces neurovascular proteases and intraventricular hemorrhage. *Sci Transl Med.* 2013;5(193):193ra90.

42. Pontes-Quero S et al. High mitogenic stimulation arrests angiogenesis. *Nat Commun.* 2019;10(1):2016.

43. Laviña B et al. Defective endothelial cell migration in the absence of Cdc42 leads to capillary-venous malformations. *Development.* 2018;145(13):dev161182.

44. Quigley JG et al. Identification of a Human Heme Exporter that Is Essential for Erythropoiesis. *Cell.* 2004;118(6):757–766.

45. Sono M, Roach MP, Coulter ED, Dawson JH. Heme-Containing Oxygenases. *Chem Rev.* 1996;96(7):2841–2888.

46. Raghuram S et al. Identification of heme as the ligand for the orphan nuclear receptors REV-ERBalpha and REV-ERBbeta. *Nat Struct Mol Biol.* 2007;14(12):1207–13.

47. Ogawa K et al. Heme mediates derepression of Maf recognition element through direct binding to transcription repressor Bach1. *EMBO J.* 2001;20(11):2835–43.

48. Jiang L et al. Bach1 represses Wnt/β-catenin signaling and angiogenesis. *Circ Res.* 2015;117(4):364–375.

49. Li M, Gallo D, Csizmadia E, Otterbein LE, Wegiel B. Carbon monoxide induces chromatin remodelling to facilitate endothelial cell migration. *Thromb Haemost.* 2014;111(5):951–959.

50. Levéen P et al. Induced disruption of the transforming growth factor beta type II receptor gene in mice causes a lethal inflammatory disorder that is transplantable. *Blood.* 2002;100(2):560–8.

51. Tian L et al. scPipe: A flexible R/Bioconductor preprocessing pipeline for single-cell RNA-sequencing data. *PLoS Comput Biol.* 2018;14(8).

52. Stuart T et al. Comprehensive Integration of Single-Cell Data. *Cell.* 2019;177(7):1888-1902.e21.

53. Moon KR et al. Visualizing structure and transitions in high-dimensional biological data. *Nat Biotechnol.* 2019;37(12):1482–1492.

54. van Dijk D et al. Recovering Gene Interactions from Single-Cell Data Using Data Diffusion. *Cell.* 2018;174(3):716-729.e27.

FIGURES

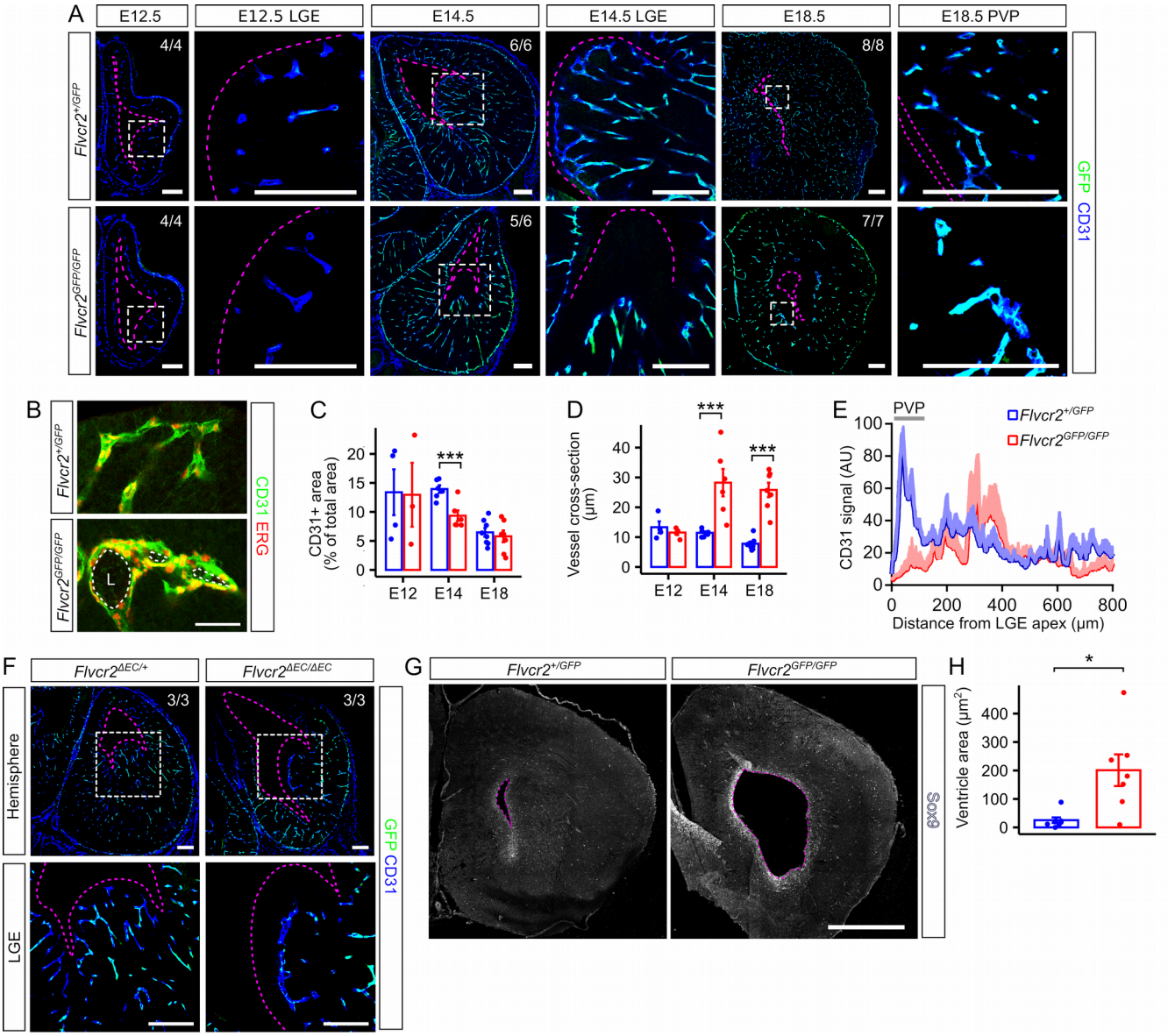

Figure 1. *Flvcr2* inactivation in mice models human PVHH. A. Coronal sections through the lateral ventricles at the indicated embryonic stages were stained to visualize GFP and the endothelial cell marker CD31. Dotted violet lines delineate the ventricles. Boxed areas show magnified areas of the lateral ganglionic eminence (LGE). Numbers indicate the number of embryos with the represented phenotype. Bars: 200 µm. **B.** Vessels in embryonic brains were stained with CD31 and ERG antibodies. A representative dilated vessel (from 5 E14.5

embryos with the phenotype) in the *Flvcr2*$^{GFP/GFP}$ GE is shown. L: vessel lumen. Bar: 50 μm. **C.** The fraction of brain area covered by CD31+ cells. ***p<0.001; t-test. E12.5 N=4; E14.5 N=6; E18.5 N=7-8. **D.** Thickness of periventricular vessels. ***p<0.001; t-test. E12.5 N=4; E14.5 N=6; E18.5 N=7-8. **E.** Fluorescence intensity profile of CD31 in the LGE of *Flvcr2*$^{+/GFP}$ and *Flvcr2*$^{GFP/GFP}$ embryos at E14.5 expressed as mean (solid line) + SEM (shaded area). N=6. **F.** Coronal sections of E14.5 brains were obtained from embryos with constitutive (*Flvcr2*$^{\Delta EC}$) deletion of Flvcr2 in endothelial cells, and stained for GFP and CD31. Bars: 200 μm. **G.** Coronal sections of E18.5 brains were stained for SOX9 (a marker of apical neuro/glia progenitors at this stage) to reveal the ventricle wall. Bars: 500 μm. **H.** Ventricle area was compared in mutants and controls. *p<0.05; t-test. *Flvcr2*$^{+/GFP}$ N=8; *Flvcr2*$^{GFP/GFP}$ N=7.

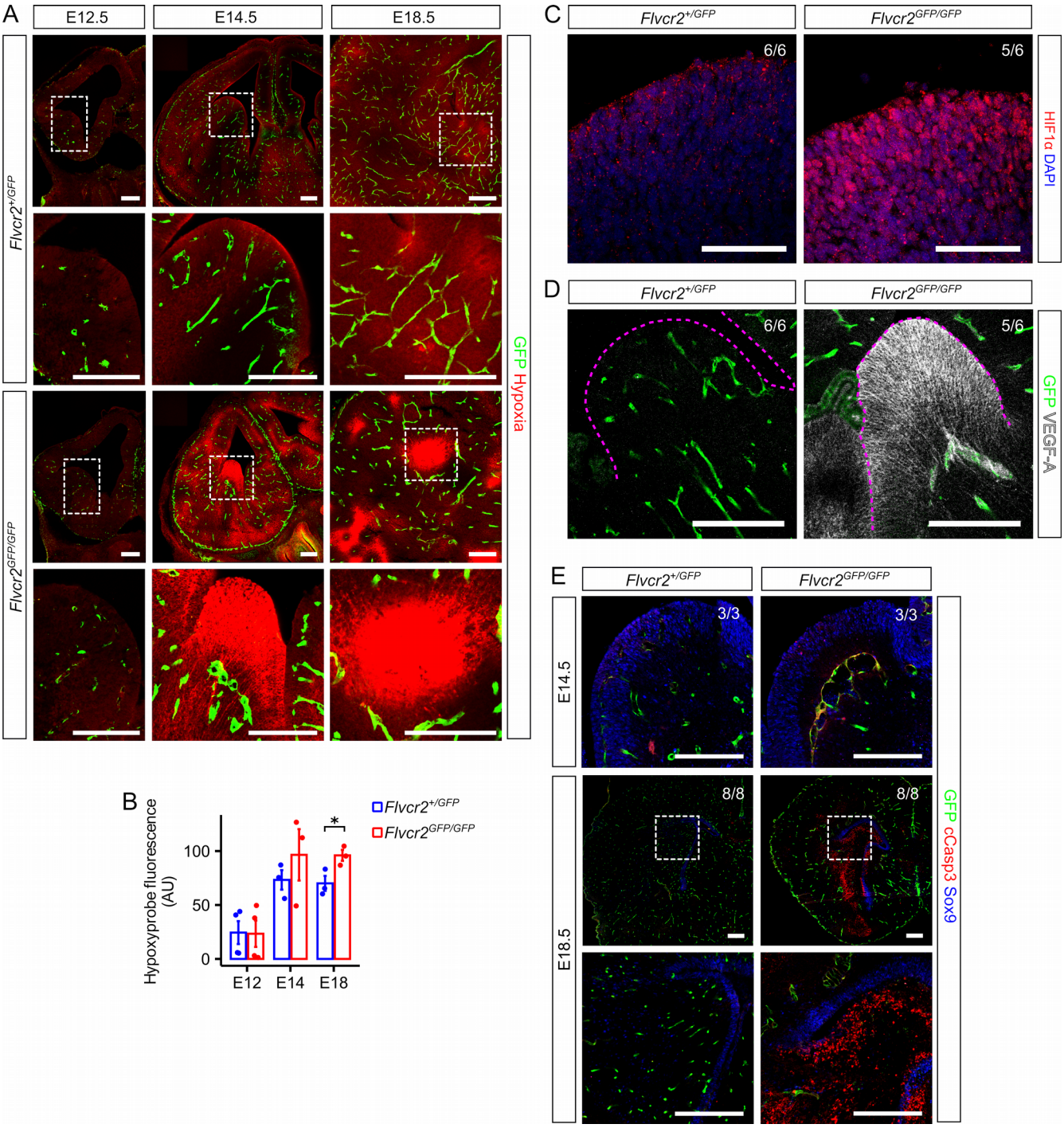

Figure 2. Brain pathology associated with *Flvcr2* deletion. A. Pregnant dams were injected with pimonidazole i.p. 3 hours before embryo collection. Pimonidazole adducts in hypoxic regions were detected in sections with a specific antibody. Bars: 200 µm. **B.** Fluorescence intensity corresponding to pimonidazole adducts was quantified in the whole

hemisphere. *p<0.05; t-test. E12.5 N=4; E14.5 N=3; E18.5 N=3. **C.** E14.5 sections containing the LGE were stained for HIF1α and DAPI. Representative images from 6 *Flvcr2*$^{+/GFP}$ and 5 *Flvcr2*$^{GFP/GFP}$ embryos. Bars: 50 μm. **D.** LGE sections were stained to reveal the presence of VEGF-A with a specific antibody. Violet dashed lines demarcate the GE. Representative images from 6 *Flvcr2*$^{+/GFP}$ and 5 *Flvcr2*$^{GFP/GFP}$ embryos. Bars: 200 μm. **E.** Coronal sections from E14.5 and E18.5 were stained for activated caspase 3 to mark dying cells. SOX9 was used to delineate the ventricular zone. Boxed regions indicate the area magnified in the lower images. Representative images from 6 *Flvcr2*$^{+/GFP}$ and 5 *Flvcr2*$^{GFP/GFP}$ embryos at E14.5, and 8 *Flvcr2*$^{+/GFP}$ and 7 *Flvcr2*$^{GFP/GFP}$ embryos at E18.5. Bars: 200 μm.

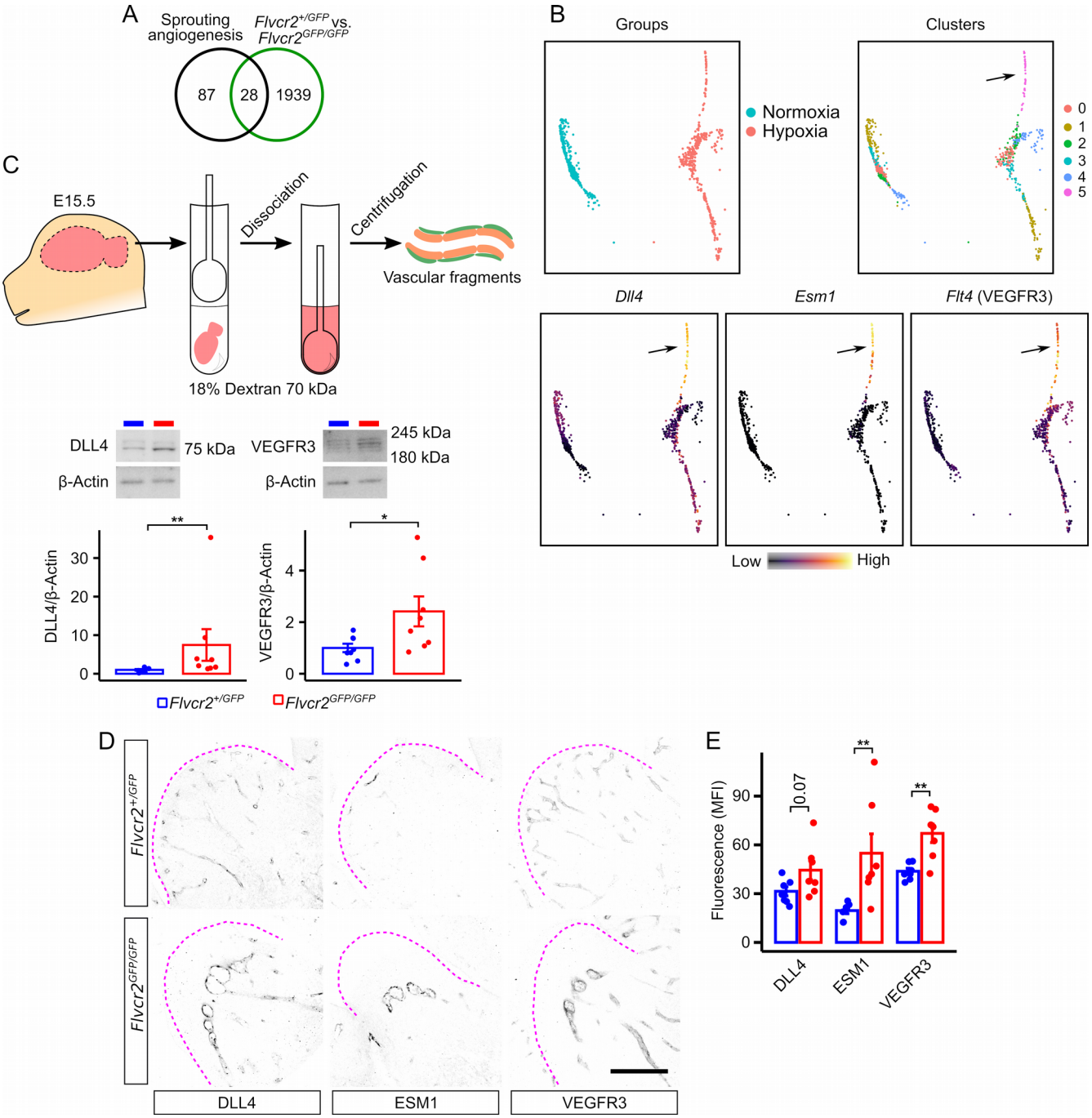

Figure 3. Angiogenesis is impaired by *Flvcr2* inactivation. A. Genes involved in sprouting angiogenesis that were differentially expressed in endothelial cells lacking *Flvcr2* are shown. N=4 per genotype. **B.** scRNA-Seq data from (27) were re-analyzed (see methods) to show expression levels of *Dll4*, *Flt4*, and *Esm1* in endothelial cells from hypoxic brains. These genes were most highly expressed in a cluster unique to the hypoxic brain (cluster 5,

indicated by arrows). **C.** Protein levels of angiogenic proteins were evaluated by western blot in brain vascular fragments from E15.5 embryos. *p<0.05, **p<0.01; t-test. N=8 per genotype. **D.** Selected proteins were detected by immunofluorescence (shown in black over white background) in sections through the LGE at E14.5. Bar: 200 μm. **E.** Fluorescence intensity of the selected proteins in Isolectin-B4+ cells was quantified. **p<0.01; t-test. N=7 per genotype.

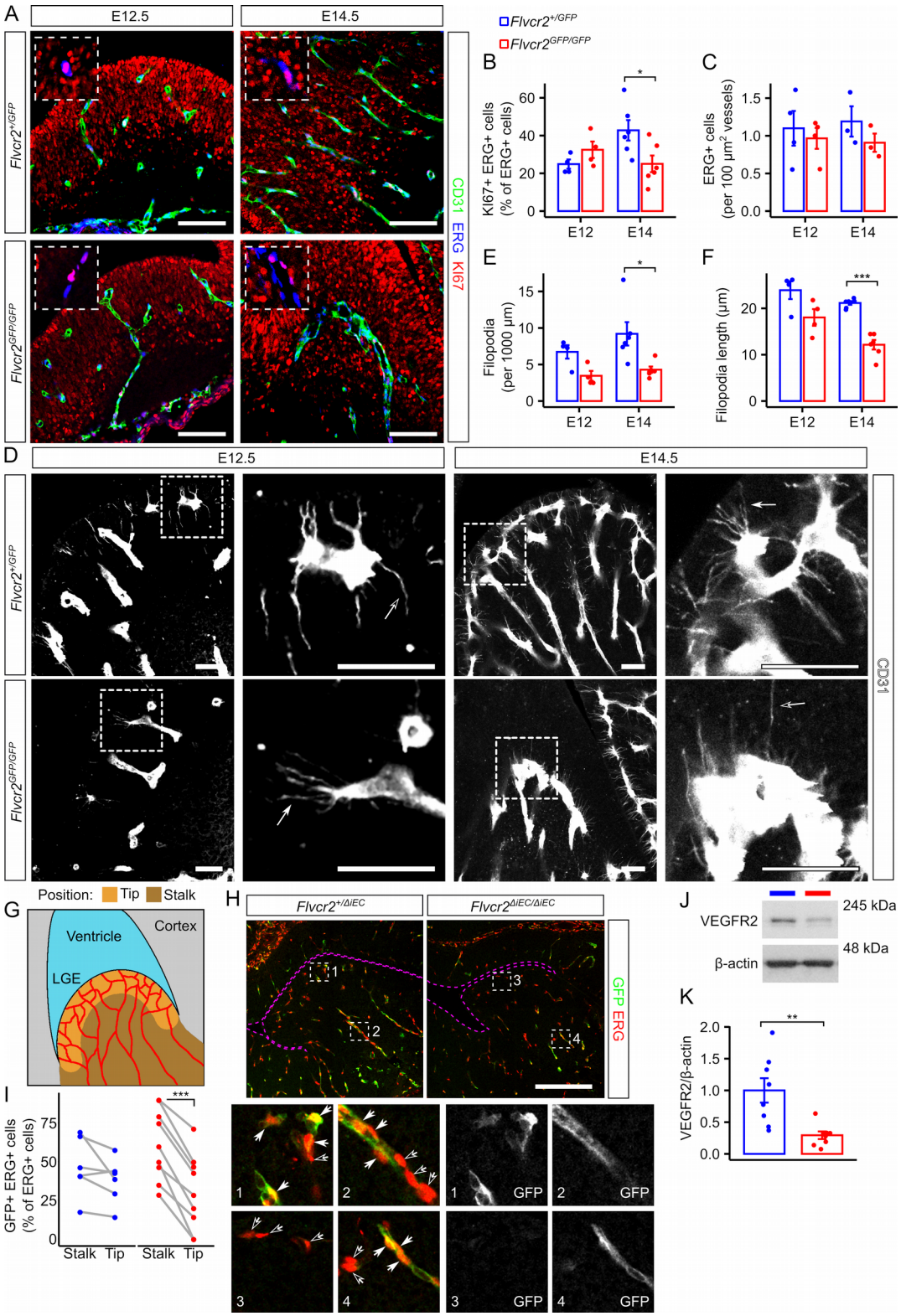

Figure 4. *Flvcr2* regulates endothelial cell sprouting in the developing brain. A. Coronal sections of the LGE at E12.5 and E14.5 were stained for CD31, the nuclear endothelial

marker ERG, and the proliferation marker KI67. Bars: 100 µm. **B.** Percentage of endothelial cells positive for the proliferation marker. E12.5 N=4; E14.5 N=6. **C.** Density of endothelial cells in the LGE. E12.5 N=4; E14.5 N=3. **D.** Coronal sections containing LGE were stained with CD31 to reveal filopodia extending from endothelial cells (arrows). Bars: 50 µm. **E.** Filopodia numbers were quantified as a function of CD31+ area at E12.5 and E14.5. *p<0.05; t-test. E12.5 N=4; E14.5 N=6. **F.** Filopodia length was measured in the same sections. ***p<0.001; t-test. E12.5 N=4; E14.5 N=6. **G.** Schematic representation of the vasculature in the LGE, highlighting presumed tip-like and stalk-like positions, based on the estimated localization of the periventricular plexus according to Fig. 1E. **H.** Mosaic recombination was induced in *Flvcr2*$^{\Delta iEC/+}$ or *Flvcr2*$^{\Delta iEC/\Delta iEC}$ embryos by daily tamoxifen injections from E10 to E12. Inactivation of the *Flvcr2* locus in endothelial cells was tracked by GFP production in ERG+ CD31+ cells. Insets show magnifications of tip- and stalk-like positions. Open arrows mark GFP- cells, while closed arrows indicate GFP+ cells. **I.** Percentage of endothelial cells lacking *Flvcr2* in the tip-like and stalk-like positions was quantified. ***p<0.001; paired t-test. *Flvcr2*$^{\Delta iEC/+}$ N=6; *Flvcr2*$^{\Delta iEC/\Delta iEC}$ N=9. **J.** VEGFR2 was detected using western blot in E15.5 brain vascular fragment homogenates from *Flvcr2*$^{+/GFP}$ (blue lanes) and *Flvcr2*$^{GFP/GFP}$ (red lanes) embryos. **K.** Quantification of VEGFR2 signal normalized to β-actin. **p<0.01; t-test. N=8 per genotype.

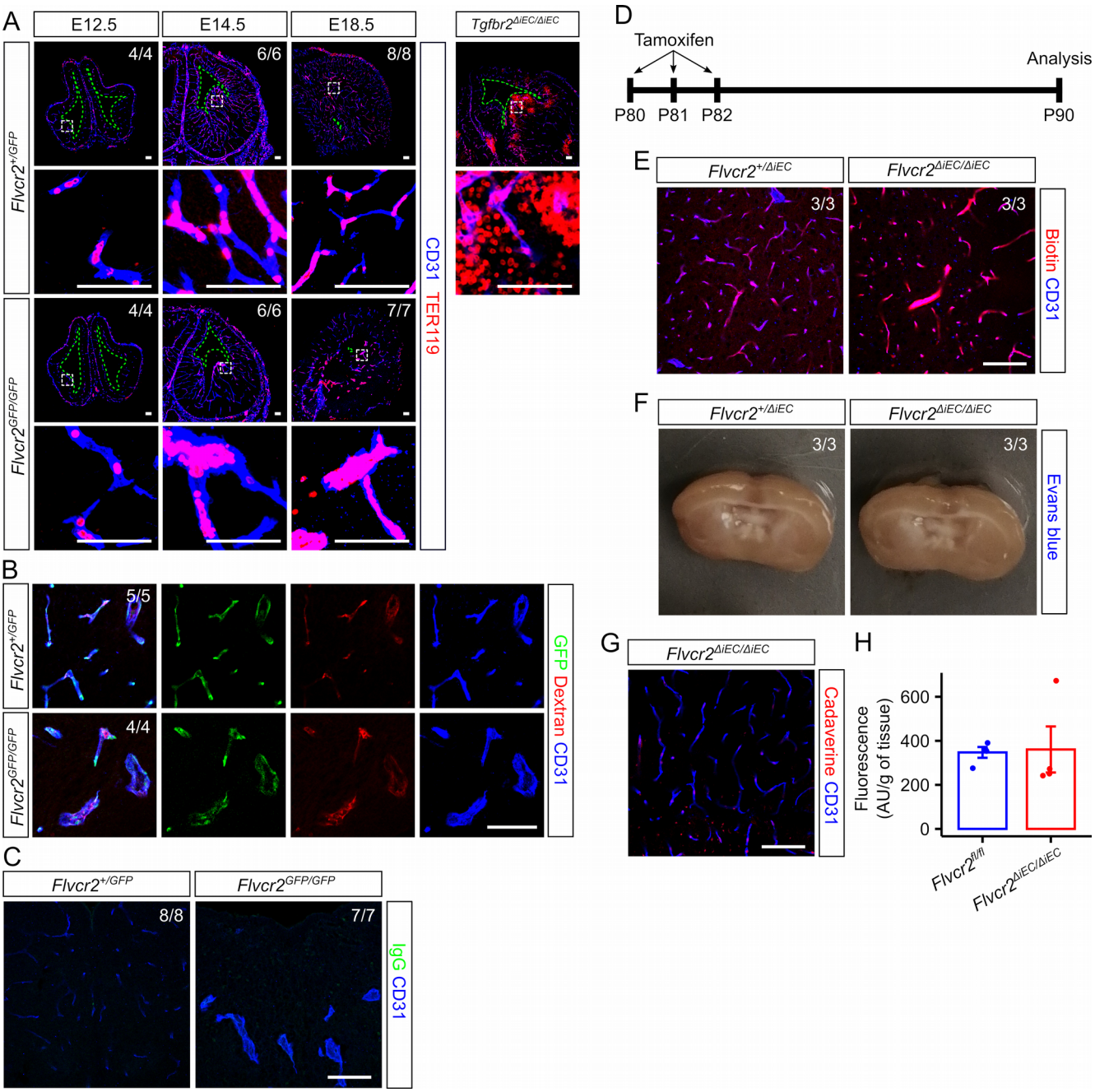

Figure 5. Blood-brain barrier is intact in *Flvcr2*$^{GFP/GFP}$ embryos. A. Red blood cells were detected in embryonic brains using an antibody against TER119. Ventricles are delineated by green dotted lines. Boxes indicate magnified areas. Hemorrhages are identified by the presence of TER119+ cells outside of CD31+ areas, as shown in *Tgfbr2*$^{\Delta iEC/\Delta iEC}$ embryos. Representative image of 2 *Tgfbr2*$^{\Delta iEC/\Delta iEC}$ embryos. Bars: 100 µm. **B.** Embryos were injected

intrahepatically with dextran 10 kDa labeled with TMR at E18.5. The fluorescence of the labeled dextran was observed in brain sections stained for GFP and CD31 to test the ability of the tracer to leak into the brain parenchyma. Bar: 100 μm. **C.** Endogenous mouse IgG was detected in brain sections at E18.5 with a fluorescently labeled antibody. Sections representative of brain parenchyma of the indicated number of embryos are shown. Bar: 100 μm. **D.** *Flvcr2* inactivation was induced by injecting tamoxifen in the indicated number of adult mice, and animals were perfused with sulfo-NHS-biotin 10 days after the last induction. Biotin presence was detected with fluorescently labeled streptavidin in brain, and localization outside of CD31+ cells was assessed. Bar: 100 μm. **E.** Recombination was induced in adult mice and Evans blue was injected i.p. 10 days later. Brains were collected after perfussion and photographed intact. N=3. **F.** Fluorescently labeled cadaverine was injected i.v. into wild-type and *Flvcr2*$^{\Delta iEC/\Delta iEC}$ mice, and brains were collected 3 hours later. The brain from one animal was sectioned to visualize dye localization. Bar: 100μm. **G.** Brains from cadaverine injected mice were homogenized and tissue fluorescence was quantified. N=4.

TABLES

Table 1. Number of wild-type, *Flvcr2*$^{+/GFP}$, and *Flvcr2*$^{GFP/GFP}$ embryos and pups recovered at different developmental stages.

Age	Wild-type	*Flvcr2*$^{+/GFP}$	*Flvcr2*$^{GFP/GFP}$
E12.5	3	5	4
E14.5	7	16	10
E18.5	7	16	9
P28	51	95	0[a]

[a]$p<0.0001$; χ^2 test.

Table 2. Number of embryos and pups from each genotype obtained from *Flvcr2*$^{fl/fl}$ x *Flvcr2*$^{fl/+}$; *Tie2-Cre* crosses.

Age	*fl/+*	*fl/+;Cre*	*fl/fl*	*fl/fl;Cre*
E12.5	9	10	11	10
E14.5	5	7	8	5
P28	32	30	44	0[a]

[a]$p<0.0001$; χ^2 test.

Table 3. Change in expression levels of genes involved in sprouting angiogenesis significantly changed in *Flvcr2*$^{GFP/GFP}$ vs. *Flvcr2*$^{+/GFP}$ embryos at E15.5.

Gene	Fold Change
Adamts9	4.82
Anxa1	3.15
Cdh13	2.36
Dll4	1.43
Eng	1.50
Epha2	2.66
Esm1	15.18
Fgfbp1	0.29
Flt1	1.85
Flt4	1.43
Hmox1	0.62
Itga5	1.45
Itgb1	1.88
Jak1	1.57
Jmjd6	1.50
Klf2	0.38
Klf4	0.38
Loxl2	3.18
Mmrn2	2.61
Nr4a1	3
Nrp1	1.74
Pgf	3.12
Plk2	1.51
Rhoj	1.89
Sema6a	0.67
Srpx2	5.33
Tbxa2r	1.57
Vegfb	0.45